Chapter 5: Reduction of Hardened Pellets by Hydrogen gas

5.1. Introduction

Carbon from coke or coal serves as the primary source of heat energy in blast furnaces and rotary hearth furnaces used worldwide. Additionally, carbon in the form of graphite electrodes is utilized in electric arc furnaces. Consequently, it's evident that carbon plays an extensive role throughout the steelmaking process, contributing significantly to global carbon dioxide (CO_2) emissions. Using hydrogen (H_2) gas as a reductant in lieu of carbonaceous material presents notable advantages, such as zero greenhouse gas (GHG) emissions, faster reduction at lower temperatures, and the absence of a complicated Boudouard (C-O) reaction system [102]. Although thermodynamics favour iron ore reduction by H_2 at temperatures higher than those achievable with CO, the smaller size of the H_2 molecule facilitates faster reduction kinetics due to its quicker diffusion. In contrast, CO molecules, being larger than H_2, diffuse more slowly into the pellet, resulting in slower reduction kinetics at lower temperatures. Consequently, hydrogen reduction occurs at temperatures lower than those required for CO [102]. Overall, the utilization of hydrogen gas as a reductant offers a promising avenue for reducing the environmental impact and enhancing the efficiency of iron production

This chapter presents a comprehensive analysis of reduction studies carried out on hardened MMO pellets utilizing pure H_2 gas. The primary aim was to optimize the time and temperature parameters for the H_2 reduction process. The MMO pellets, containing 1.5 wt.% colemanite, underwent reduction within the temperature range of 700-900 °C for durations ranging from 1 to 60 mins. Three different gas flow rates, namely 0.25 L/min, 0.5 L/min, and 1 L/min, were examined. A notable observation was the occurrence of cracking and subsequent decline in the CCS of MMO pellets post-reduction. XRD and SEM analysis of the reduced MMO pellets revealed a significant influence of gangue elements on the CCS of the pellets. Subsequently, the impact of

gangue elements was investigated by fabricating synthetic pellets. These synthetic pellets were evaluated for their CCS both before and after reduction. Furthermore, characterization of the synthetic pellets was carried out using XRD and SEM techniques.

5.2. Results and Discussion

5.2.1. Reduction Studies

Reduction of the hardened MMO pellets was carried out according to methods mentioned in Section 2.6.2 of Chapter 2. The MMO pellet's weight before and after reduction were recorded to calculate the weight change. The weight change of the pellet was used to calculate the Degree of Reduction (% R) as

%R = (Change in wt. of pellet/ Wt. of removable oxygen present in Initial pellet) × 100…….(5.1)

The weight of removable oxygen was determined by considering the oxygen associated with the oxides in the MMO pellets which can be readily reduced by H_2 within the temperature range of 700-900 °C. A negative ΔG_r of the reduction reaction within the specified temperature range indicates spontaneous reduction of the oxide. The ΔG_r for reduction of Fe_2O_3 to Fe_3O_4, Fe_3O_4 to FeO, FeO to Fe and NiO to Ni by Hydrogen gas in the temperature range of 700-900 °C lies between -91.99 KJ to -109.88 KJ, -19.37 KJ to -30.58 KJ, 14.56 KJ to 13.13 KJ and -42.46 KJ to -48.39 KJ, respectively, which was calculated using FactSage software [93]**.** Though the ΔG_r for FeO to Fe is positive but the ΔG_r for complete reduction of Fe_2O_3 to Fe in the temperature range of 700-900 °C ranges between -14.69 KJ to -30.68 KJ. Chromite is not reducible by H_2 at the temperatures used in these experiments. Thus, for the calculation of % R, only the oxygen associated with Fe and Ni was considered as the total removable oxygen, which amounts to 17.23% of the pellet weight. Therefore, eqn. 5.1 can be rewritten as follows

%R= (Change in wt. of pellet/ 0.1723 *initial wt. of pellet) × 100……(5.2)

In cases where the % R for a longer reduction time and lower flow rate equals the % R achieved with a shorter reduction time and higher flow rate, determining the optimum conditions for reduction can be challenging. In such circumstances, % H_2 utilization becomes crucial for assessing the efficiency of the gas utilization for reduction process. Thus the % H_2 utilization was calculated to get an idea of how frugally the supplied hydrogen gas was being utilized in the reduction reaction. This was done in the following way. It was assumed that all oxygen lost, combined with hydrogen gas to form water. Based on the above mentioned assumption, the amount of hydrogen required for % R=100 was calculated. For % R =100, the **wt. of hydrogen gas required** is (2 × Wt. of removable oxygen)/16. Now, for actual % R for an experiment, the **wt. of hydrogen consumed in the experiment** is given by (wt. of hydrogen gas required × %R) /100. Thus, the amount of hydrogen gas utilized (% H_2 utilization) is calculated as

% H_2 utilization= (wt. of hydrogen consumed in the experiment / wt. of hydrogen supplied) × 100…….(5.3)

5.2.1.1. Reduction at 700 °C

The % R obtained with change in reduction time at reduction temperature of 700 °C is shown in **Table 5.1**.

Table 5.1: Percentage Reducation (% R) with change in reduction time and gas flow rate at 700 °C.

Flow rate (L/min)	Reduction Time (mins)	Initial wt of pellets(gm)	Final wt of pellets(gm)	Wt. change (gm)	Wt. of removable Oxygen (gm)	%R
0.25	1	20.348	20.201	0.147	3.506	4.185
	3	19.428	19.032	0.396	3.347	11.828
	5	20.154	19.494	0.660	3.473	19.003
	10	21.974	20.987	0.987	3.786	26.070
	15	20.597	19.162	1.435	3.549	40.425
	20	22.234	20.406	1.828	3.831	47.727
	30	20.435	18.066	2.369	3.521	67.287
	45	21.068	18.551	2.517	3.630	69.330
	50	21.548	18.942	2.605	3.715	70.126
	60	22.879	20.112	2.767	3.944	70.140
0.5	1	19.954	19.675	0.279	3.438	8.104
	3	20.030	19.379	0.651	3.451	18.855
	5	19.831	18.991	0.840	3.417	24.569
	10	19.792	18.288	1.504	3.410	44.102
	15	22.596	20.624	1.972	3.893	50.659
	20	21.030	18.527	2.503	3.623	69.076
	30	20.722	18.138	2.585	3.570	72.387
	45	20.515	17.679	2.836	3.535	80.222
	50	21.180	18.230	2.950	3.649	80.850
	60	24.885	21.409	3.476	4.288	81.065
1	1	20.167	19.792	0.375	3.475	10.788
	3	20.269	19.353	0.916	3.492	26.217
	5	21.033	19.609	1.424	3.624	39.300
	10	18.843	16.706	2.137	3.247	65.830
	15	19.921	17.555	2.366	3.432	68.943
	20	20.213	17.554	2.659	3.483	76.341
	30	18.853	16.124	2.729	3.248	84.021
	45	19.113	16.333	2.780	3.293	84.408
	50	22.860	19.529	3.331	3.939	84.560
	60	22.140	18.899	3.241	3.815	84.950

The degree of metallization (% Fe_M) in pellets reduced at 700 °C was calculated according to the methods mentioned in Section 2.6.3 of Chapter 2 and is shown in **Table 5.2.**

Table 5.2: Percentage Metallization (% Fe_M) with change in reduction time and gas flow rate at 700°C

Flow rate (L/min)	Reduction Time (mins)	Initial wt. of pellet (gm)	Wt. of DRI (gm)	$K_2Cr_2O_7$ Solution consumed (ml)	Initial wt. of Iron in pellet (gm)	Fe per gm DRI Fe(T) (gm)	Fe(M) (gm)	Fe_M(%)
0.25	1	20.348	20.201	0.400	9.177	0.454	0.001	0.171
	3	19.428	19.032	2.100	8.762	0.460	0.004	0.855
	5	20.154	19.494	4.300	9.089	0.466	0.008	1.711
	10	21.974	20.987	8.700	9.910	0.472	0.016	3.421
	15	20.597	19.162	44.500	9.289	0.485	0.083	17.106
	20	22.234	20.406	90.300	10.028	0.491	0.168	34.212
	30	20.435	18.066	145.300	9.216	0.510	0.271	53.029
	45	21.068	18.551	174.100	9.502	0.512	0.324	63.293
	50	21.548	18.942	179.800	9.718	0.513	0.335	65.250
	60	22.879	20.112	180.300	10.318	0.513	0.336	65.420
0.5	1	19.954	19.675	8.400	8.999	0.457	0.016	3.421
	3	20.030	19.379	17.100	9.034	0.466	0.032	6.842
	5	19.831	18.991	34.600	8.944	0.471	0.064	13.685
	10	19.792	18.288	76.200	8.926	0.488	0.142	29.080
	15	22.596	20.624	95.300	10.191	0.494	0.178	35.923
	20	21.030	18.527	145.800	9.485	0.512	0.271	53.029
	30	20.722	18.138	175.100	9.346	0.515	0.326	63.293
	45	20.515	17.679	211.500	9.252	0.523	0.394	75.267
	50	21.180	18.230	212.900	9.552	0.524	0.396	75.650
	60	24.885	21.409	215.400	11.223	0.524	0.401	76.520
1	1	20.167	19.792	10.600	9.095	0.460	0.020	4.277
	3	20.269	19.353	19.500	9.141	0.472	0.036	7.698
	5	21.033	19.609	44.400	9.486	0.484	0.083	17.106
	10	18.843	16.706	144.900	8.498	0.509	0.270	53.029
	15	19.921	17.555	159.900	8.984	0.512	0.298	58.161
	20	20.213	17.554	185.100	9.116	0.519	0.345	66.372
	30	18.853	16.124	203.500	8.503	0.527	0.379	71.846
	45	19.113	16.333	223.000	8.620	0.528	0.415	78.688
	50	22.860	19.529	223.900	10.310	0.528	0.417	78.980
	60	22.140	18.899	224.600	9.985	0.528	0.418	79.150

The % H_2 utilization at 700 °C was calculated according to **eqn. 5.3** and is shown in **Table 5.3**.

Table 5.3: % H_2 utilization with change in reduction time and gas flow rate at 700°C

Flow rate (L/min)	Reduction time (mins)	Wt. of removable Oxygen (gm)	Hydrogen supplied (L)	Hydrogen supplied (gm)	%R	Hydrogen consumed (gm)	% H_2 utilization
0.25	1	3.506	0.250	0.020	4.185	0.018	89.680
	3	3.347	0.750	0.061	11.828	0.049	80.672
	5	3.473	1.250	0.102	19.003	0.082	80.672
	10	3.786	2.500	0.204	26.070	0.123	60.336
	15	3.549	3.750	0.307	40.425	0.179	58.463
	20	3.831	5.000	0.409	47.727	0.229	55.882
	30	3.521	7.500	0.613	67.287	0.296	48.273
	45	3.630	11.250	0.920	69.330	0.315	34.186
	50	3.715	12.500	1.022	70.126	0.326	31.848
	60	3.944	15.000	1.227	70.140	0.346	28.185
0.5	1	3.438	0.500	0.041	8.104	0.035	85.154
	3	3.451	1.500	0.123	18.855	0.081	66.293
	5	3.417	2.500	0.204	24.569	0.105	51.317
	10	3.410	5.000	0.409	44.102	0.188	45.966
	15	3.893	7.500	0.613	50.659	0.247	40.187
	20	3.623	10.000	0.818	69.076	0.313	38.249
	30	3.570	15.000	1.227	72.387	0.323	26.331
	45	3.535	22.500	1.840	80.222	0.354	19.259
	50	3.649	25.000	2.045	80.850	0.369	18.035
	60	4.288	30.000	2.454	81.065	0.434	17.706
1	1	3.475	1.000	0.082	10.788	0.047	57.283
	3	3.492	3.000	0.245	26.217	0.114	46.639
	5	3.624	5.000	0.409	39.300	0.178	43.529
	10	3.247	10.000	0.818	65.830	0.267	32.661
	15	3.432	15.000	1.227	68.943	0.296	24.108
	20	3.483	20.000	1.636	76.341	0.332	20.315
	30	3.248	30.000	2.454	84.021	0.341	13.903
	45	3.293	45.000	3.681	84.408	0.347	9.440
	50	3.939	50.000	4.090	84.560	0.416	10.180
	60	3.815	60.000	4.908	84.950	0.405	8.254

The values of %R, % Fe_M and % H_2 utilization obtained in **Table 5.1, 5.2 and 5.3** are plotted against reduction time and shown in **Figure 5.1**.

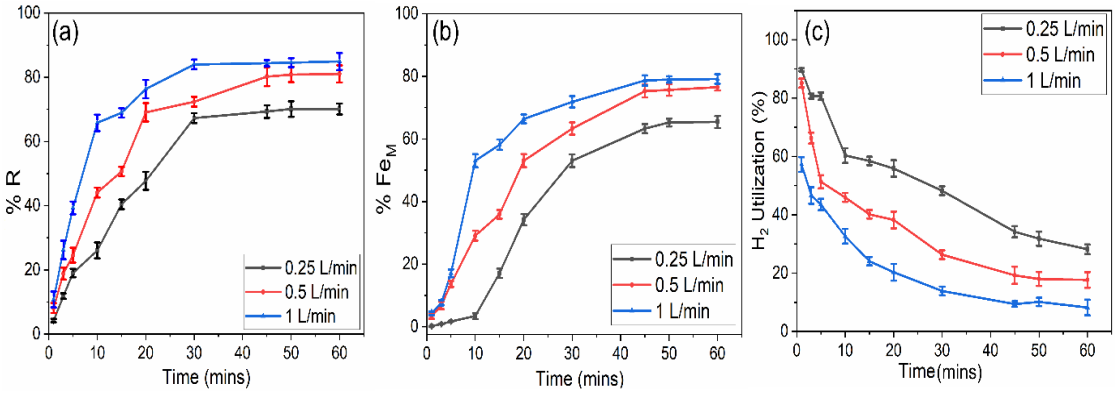

Figure 5.1: Variation of (a) % Reduction (b) % Metallization (c) % H_2 utilization; with time at 700 °C

At 700 °C, the maximum possible % R, % Fe_M was 84.95% and 75.15% respectively, which was attained at a gas flow rate of 1 L/min and a reduction time of 60 mins. However, the % H_2 utilization in the above-mentioned conditions was a dismal 9.01%, which indicated that maximum gas passed out of the reduction chamber unutilized. In general, % R and % Fe_M values were found to increase with increase in flow rate. The % H_2 utilization decreased monotonically with increased flow rates. An increase in flow rate leads to increased hydrogen gas near the pellet surface, thereby speeding up the chemical reaction and increasing reducibility.

The % R reached a plateau at approximately 65%, 75%, and 80% after 30 mins for flow rates of 0.25 L/min, 0.5 L/min, and 1 L/min, respectively. To investigate this phenomenon, pellets were sectioned longitudinally into two halves. One half of each pellet underwent careful examination from surafce towards the centre, under a scanning electron microscope (SEM) at a magnification of 100X. Area scans were performed on the peripheral region and centre of pellets reduced at flow rates of 0.25 L/min, 0.5 L/min, and 1 L/min using SEM-EDS to determine the elemental composition. The results of these area scans are presented in **Table 5.4**. Subsequently, the oxygen

contents obtained from **Table 5.4** are plotted against reduction time (**Figure 5.2**) to understand the variation of oxygen between the surface and the centre of the pellets.

Table 5.4: Elemental Compositions of area scans

Flow rate (L/min)	Area of pellet scanned	Reduction Time (mins)	Element				
			O	Al	Si	Cr	Fe
0.25	Side	20	23.59	6.21	6.44	4.21	59.55
		30	19.14	7.12	7.22	5.05	61.47
		45	18.6	7.11	6.95	5.25	62.09
	Centre	20	28.22	6.89	6.84	4.19	53.86
		30	27.56	6.59	6.27	4.22	55.36
		45	27.55	6.43	6.42	4.18	55.42
0.5	Side	20	19.52	7.06	6.89	4.24	62.29
		30	17.67	7.22	6.47	4.85	63.79
		45	16.18	7.19	7.45	5.15	64.03
	Centre	20	27.84	6.65	5.96	4.82	54.73
		30	26.86	6.91	6.67	4.23	55.33
		45	26.78	6.22	6.13	4.18	56.69
1	Side	20	17.14	6.84	6.3	5.81	63.91
		30	15.82	7.02	6.65	5.05	65.46
		45	15.15	6.93	7.05	5.13	65.74
	Centre	20	26.98	6.69	6.58	4.12	55.63
		30	25.86	6.57	6.36	4.07	57.14
		45	25.75	6.37	6.15	3.75	57.98

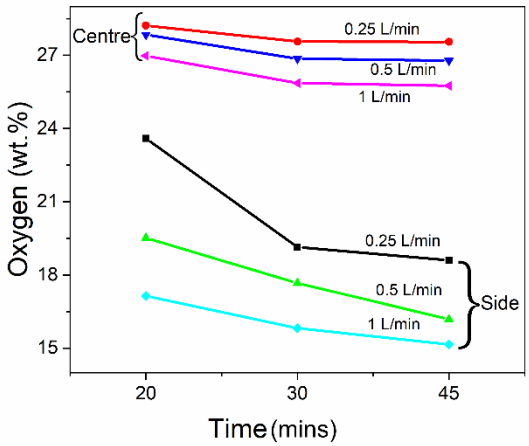

Figure 5.2 Variation of Oxygen content at the side and centre of pellet with respect to reduction time and flow rate of hydrogen

The decrease in wt. % of oxygen on the side of the pellet with an increase in reduction time was more, as compared to the centre of the pellet at all flow rates (**Figure 5.2 and Table 5.4**). It shows that the hydrogen atoms could not diffuse deep into the pellet due to lower kinetic energy of the atoms at lower temperature. Increasing the flow rate only served to increase the rate of chemical reaction in the surface of the pellets. The increase

in flow rates led to higher concentrations of gas atoms close to pellets and a decrease in gas starvation conditions.

5.2.1.2. Reduction at 800 °C

The % R obtained with change in reduction time at reduction temperature of 800 °C is shown in **Table 5.5**.

Table 5.5: Percentage Reduction (% R) with change in reduction time and gas flow rate at 800 °C.

Flow rate (L/min)	Reduction Time (mins)	Initial wt. of pellets (gm)	Final wt. of pellets (gm)	Wt. change (gm)	Wt. of removable Oxygen (gm)	%R
0.25	1	20.210	20.062	0.148	3.482	4.237
	3	21.160	20.725	0.435	3.646	11.940
	5	19.972	19.260	0.712	3.441	20.694
	10	21.206	19.842	1.364	3.654	37.329
	15	20.583	18.685	1.898	3.546	53.520
	20	20.801	18.697	2.104	3.584	58.712
	30	21.519	18.837	2.682	3.708	72.326
	45	20.016	17.132	2.884	3.449	83.630
	50	21.756	18.605	3.151	3.749	84.065
	60	23.721	20.283	3.438	4.087	84.122
0.5	1	20.951	20.657	0.294	3.610	8.150
	3	20.291	19.513	0.778	3.496	22.256
	5	22.295	21.043	1.252	3.841	32.590
	10	20.497	18.904	1.593	3.532	45.103
	15	22.083	19.721	2.362	3.805	62.069
	20	19.489	16.882	2.607	3.358	77.649
	30	20.568	17.521	3.047	3.544	85.989
	45	21.409	18.174	3.235	3.689	87.699
	50	22.015	18.658	3.357	3.793	88.501
	60	22.002	18.625	3.377	3.791	89.081
1	1	19.857	19.369	0.488	3.421	14.251
	3	19.820	18.590	1.230	3.415	36.016
	5	21.653	19.572	2.081	3.731	55.788
	10	20.176	17.443	2.733	3.476	78.617
	15	20.237	17.249	2.988	3.487	85.687
	20	19.466	16.496	2.970	3.354	88.561
	30	18.399	15.530	2.869	3.170	90.488
	45	18.869	15.882	2.987	3.251	91.871
	50	22.597	19.032	3.565	3.893	91.560
	60	21.951	18.476	3.475	3.782	91.880

The degree of metallization (% Fe_M) in pellets reduced at 800 °C was calculated according to the methods mentioned in Section 2.6.3 of Chapter 2 and is shown in **Table 5.6.**

Table 5.6: Percentage Metallization (%Fe_M) with change in reduction time and gas flow rate at 800°C

Flow rate (L/min)	Reduction Time (mins)	Initial wt. of pellet (gm)	Wt. of DRI (gm)	$K_2Cr_2O_7$ Solution consumed (ml)	Initial wt. of Iron in pellet (gm)	Fe per gm DRI Fe(T) (gm)	Fe(M) (gm)	Fe_M(%)
0.25	1	20.210	20.062	1.700	9.115	0.454	0.003	0.684
	3	21.160	20.725	2.100	9.543	0.460	0.004	0.855
	5	19.972	19.260	8.200	9.007	0.468	0.015	3.250
	10	21.206	19.842	53.100	9.564	0.482	0.099	20.527
	15	20.583	18.685	73.000	9.283	0.497	0.136	27.370
	20	20.801	18.697	124.500	9.381	0.502	0.232	46.187
	30	21.519	18.837	151.500	9.705	0.515	0.282	54.740
	45	20.016	17.132	213.000	9.027	0.527	0.397	75.267
	50	21.756	18.605	215.600	9.812	0.527	0.401	76.125
	60	23.721	20.283	215.700	10.698	0.527	0.402	76.144
0.5	1	20.951	20.657	16.800	9.449	0.457	0.031	6.842
	3	20.291	19.513	21.500	9.151	0.469	0.040	8.553
	5	22.295	21.043	35.100	10.055	0.478	0.065	13.685
	10	20.497	18.904	89.800	9.244	0.489	0.167	34.212
	15	22.083	19.721	125.300	9.959	0.505	0.233	46.187
	20	19.489	16.882	191.300	8.790	0.521	0.356	68.424
	30	20.568	17.521	214.000	9.276	0.529	0.398	75.267
	45	21.409	18.174	239.200	9.655	0.531	0.445	83.820
	50	22.015	18.658	240.100	9.929	0.532	0.447	84.012
	60	22.002	18.625	240.400	9.923	0.533	0.448	84.021
1	1	19.857	19.369	17.000	8.956	0.462	0.032	6.842
	3	19.820	18.590	25.600	8.939	0.481	0.048	9.922
	5	21.653	19.572	105.400	9.766	0.499	0.196	39.344
	10	20.176	17.443	177.300	9.099	0.522	0.330	63.293
	15	20.237	17.249	221.200	9.127	0.529	0.412	77.833
	20	19.466	16.496	234.700	8.779	0.532	0.437	82.109
	30	18.399	15.530	249.400	8.298	0.534	0.464	86.899
	45	18.869	15.882	256.000	8.510	0.536	0.477	88.952
	50	22.597	19.032	257.200	10.191	0.535	0.479	89.450
	60	21.951	18.476	257.300	9.900	0.536	0.479	89.410

The % H_2 utilization with change in reduction time at 800 °C was calculated according to **eqn. 5.3** and is shown in **Table 5.7.**

Table 5.7: Variation of % H_2 utilization with change in reduction time and gas flow rate at 800°C

Flow rate (L/min)	Reduction Time (mins)	Wt. of removable Oxygen (gm)	Hydrogen supplied (L)	Hydrogen supplied (gm)	%R	Hydrogen consumed (gm)	% H_2 utilization
0.25	1	3.482	0.250	0.020	4.237	0.018	90.196
	3	3.646	0.750	0.061	11.940	0.054	88.702
	5	3.441	1.250	0.102	20.694	0.089	87.059
	10	3.654	2.500	0.204	37.329	0.170	83.373
	15	3.546	3.750	0.307	53.520	0.237	77.348
	20	3.584	5.000	0.409	58.712	0.263	64.314
	30	3.708	7.500	0.613	72.326	0.335	54.641
	45	3.449	11.250	0.920	83.630	0.361	39.178
	50	3.749	12.500	1.022	84.065	0.394	38.526
	60	4.087	15.000	1.227	84.122	0.430	35.028
0.5	1	3.610	0.500	0.041	8.150	0.037	89.916
	3	3.496	1.500	0.123	22.256	0.097	79.272
	5	3.841	2.500	0.204	32.590	0.156	76.527
	10	3.532	5.000	0.409	45.103	0.199	48.684
	15	3.805	7.500	0.613	62.069	0.295	48.120
	20	3.358	10.000	0.818	77.649	0.326	39.846
	30	3.544	15.000	1.227	85.989	0.381	31.046
	45	3.723	22.500	1.840	87.699	0.404	21.972
	50	3.831	25.000	2.045	88.501	0.420	20.520
	60	4.136	30.000	2.454	89.081	0.422	17.202
1	1	3.421	1.000	0.082	14.251	0.061	74.510
	3	3.415	3.000	0.245	36.016	0.154	62.652
	5	3.731	5.000	0.409	55.788	0.260	63.614
	10	3.476	10.000	0.818	78.617	0.342	41.765
	15	3.487	15.000	1.227	85.687	0.373	30.439
	20	3.354	20.000	1.636	88.561	0.371	22.696
	30	3.170	30.000	2.454	90.488	0.359	14.613
	45	3.251	45.000	3.681	91.871	0.373	10.143
	50	3.893	50.000	4.090	91.560	0.446	10.896
	60	3.782	60.000	4.908	91.880	0.434	8.851

The values of %R, % Fe_M and % H_2 utilization obtained in **Table 5.5, 5.6 and 5.7** are plotted against reduction time and shown in **Figure 5.3**

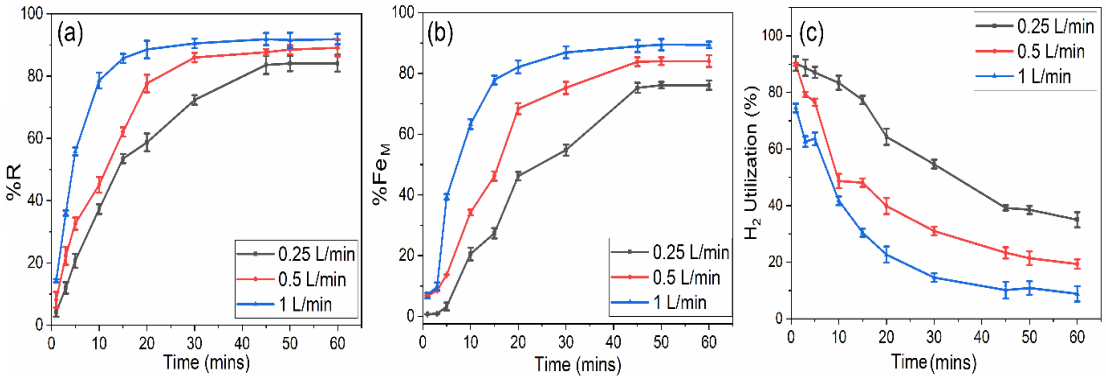

Figure 5.3: Variation of (a) % Reduction (b) % Metallization (c) % H_2 utilization; with time at 800 °C

In general, % R and % Fe_M values were found to increase with increase in flow rate. The % H_2 utilization decreased monotonically with increase of flow rates. An increase in flow rate leads to increase in hydrogen gas near the pellet surface, thereby speeding up the chemical reaction and increasing %R. At 800 °C, the maximum possible %R and % Fe_M was 91.88 % and 89.41 % respectively, which was attained at a gas flow rate of 1 L/min and a reduction time of 60 mins. At the aforementioned flow rates and reduction times, the %R and % Fe_M increased about 8.2 % and 13% respectively, when the temperature was increased from 700°C to 800 °C (**Figure 5.1 and 5.3**). Similar observations of an increase in the % R have been reported in other studies[61, 102]. The increase in % R was attributed to the accelerated diffusion rate of H_2 gas. This enhanced diffusion rate allowed hydrogen to permeate the iron pellets more rapidly, facilitating more efficient reduction reactions. However, the % H_2 utilization in the above mentioned conditions was a dismal 8.85%, which indicated that maximum gas passed out of the reduction chamber unutilized. In contrast % R, % Fe_M and % H_2 utilization of about 91%, 84% and 24% was achieved after 30 mins at a reduced gas flow rate of 0.5 L/min. This indicates that increasing the flow rate beyond 0.5 L/min at 800 °C had negligible impact on the maximum possible %R of pellets. It can also be observed that the maximum % R and maximum % Fe_M do not change much on

increasing the reduction time at flow rate of 0.5 L/min. Increasing the flow rate from 0.25 L/min to 0.5 L/min increased both the maximum % R and % Fe_M, but the same effect was not observed when flow rate was increased to 1 L/min from 0.5L/min.

5.2.1.3. Reduction at 900 °C

The % R obtained with change in reduction time at a reduction temperature of 900 °C is shown in Table 5.8, respectively.

Table 5.8 : Percentage Reduction (% R) with change in reduction time and gas flow rate at 900 °C.

Flow rate (L/min)	Reduction Time (mins)	Initial wt of pellets (gm)	Final wt of pellets (gm)	Wt. change (gm)	Wt. of removable Oxygen (gm)	%R
0.25	1	17.700	17.551	0.149	3.050	4.898
	3	19.247	18.803	0.444	3.316	13.404
	5	21.849	21.116	0.733	3.765	19.476
	10	19.507	18.138	1.369	3.361	40.738
	15	19.360	17.417	1.943	3.336	58.247
	20	19.620	17.401	2.219	3.381	65.635
	30	23.052	20.070	2.982	3.972	75.085
	45	19.869	16.802	3.067	3.423	89.596
	50	21.608	18.273	3.067	3.423	89.558
	60	22.917	19.376	3.542	3.949	89.695
0.5	1	18.628	18.332	0.296	3.210	9.223
	3	19.263	18.434	0.829	3.319	24.962
	5	19.882	18.653	1.229	3.426	35.877
	10	19.449	17.514	1.935	3.351	57.734
	15	19.329	16.846	2.483	3.330	74.549
	20	20.118	17.192	2.926	3.466	84.412
	30	19.361	16.468	2.893	3.336	86.736
	45	20.800	17.510	3.290	3.584	91.799
	50	22.455	18.919	3.536	3.869	91.392
	60	23.230	19.546	3.684	4.003	92.042
1	1	19.302	18.756	0.546	3.326	16.424
	3	19.191	17.907	1.284	3.307	38.831
	5	20.023	17.920	2.103	3.450	60.954
	10	18.859	16.228	2.631	3.249	80.976
	15	19.313	16.318	2.995	3.328	89.990
	20	21.270	17.917	3.353	3.665	91.503
	30	20.112	16.887	3.225	3.465	93.069
	45	21.011	17.629	3.382	3.620	93.409
	50	21.772	18.246	3.526	3.751	93.986
	60	21.855	18.313	3.542	3.766	94.072

The % metallization (% Fe_M) in pellets reduced at 900 °C was calculated according to the methods mentioned in Section 2.6.3 of Chapter 2 and is shown in **Table 5.9.**

Table 5.9: Percentage Metallization (%Fe_M) with change in reduction time and gas flow rate at 900°C

Flow rate (L/min)	Reduction Time (mins)	Initial wt. of pellet (gm)	Wt. of DRI (gm)	$K_2Cr_2O_7$ Solution consumed (ml)	Initial wt. of Iron in pellet (gm)	Fe per gm DRI Fe(T) (gm)	Fe(M) (gm)	Fe_M(%)
0.25	1	17.700	17.551	2.100	7.983	0.455	0.004	0.855
	3	19.247	18.803	2.500	8.680	0.462	0.005	1.026
	5	21.849	21.116	8.600	9.854	0.467	0.016	3.421
	10	19.507	18.138	44.600	8.798	0.485	0.083	17.106
	15	19.360	17.417	92.100	8.731	0.501	0.172	34.212
	20	19.620	17.401	154.200	8.849	0.509	0.287	56.450
	30	23.052	20.070	192.800	10.396	0.518	0.359	69.293
	45	19.869	16.802	254.800	8.961	0.533	0.474	88.952
	50	21.608	18.273	254.700	9.745	0.533	0.474	88.941
	60	22.917	19.376	254.100	10.336	0.533	0.473	88.700
0.5	1	18.628	18.332	16.800	8.401	0.458	0.031	6.842
	3	19.263	18.434	28.600	8.688	0.471	0.053	11.290
	5	19.882	18.653	57.400	8.967	0.481	0.107	22.238
	10	19.449	17.514	133.400	8.771	0.501	0.248	49.608
	15	19.329	16.846	190.200	8.717	0.517	0.354	68.424
	20	20.118	17.192	218.200	9.073	0.528	0.406	76.977
	30	19.361	16.468	250.400	8.732	0.530	0.466	87.925
	45	20.800	17.510	261.700	9.381	0.536	0.487	90.952
	50	22.455	18.919	261.400	10.127	0.535	0.487	90.941
	60	23.230	19.546	261.100	10.477	0.536	0.486	90.700
1	1	19.302	18.756	21.300	8.705	0.464	0.040	8.553
	3	19.191	17.907	36.400	8.655	0.483	0.068	14.027
	5	20.023	17.920	141.700	9.030	0.504	0.264	52.345
	10	18.859	16.228	199.800	8.505	0.524	0.372	70.990
	15	19.313	16.318	243.700	8.710	0.534	0.454	85.017
	20	21.270	17.917	249.400	9.593	0.535	0.464	86.728
	30	20.112	16.887	259.500	9.071	0.537	0.483	89.952
	45	21.011	17.629	266.700	9.476	0.538	0.497	92.373
	50	21.772	18.246	266.200	9.819	0.538	0.496	92.120
	60	21.855	18.313	267.200	9.857	0.538	0.498	92.450

The % H_2 utilization at 900 °C was calculated according to **eqn. 5.3** and is shown in **Table 5.10.**

Table 5.10: % H_2 utilization with change in reduction time and gas flow rate at 900°C

Flow rate (L/min)	Reduction Time (mins)	Wt. of removable Oxygen (gm)	Hydrogen supplied (L)	Hydrogen supplied (gm)	%R	Hydrogen consumed (gm)	% H_2 utilization
0.25	1	3.050	0.250	0.020	4.898	0.019	91.317
	3	3.316	0.750	0.061	13.404	0.056	90.570
	5	3.765	1.250	0.102	19.476	0.092	89.636
	10	3.361	2.500	0.204	40.738	0.171	83.698
	15	3.336	3.750	0.307	58.247	0.243	79.178
	20	3.381	5.000	0.409	65.635	0.277	67.815
	30	3.972	7.500	0.613	75.085	0.373	60.766
	45	3.423	11.250	0.920	89.596	0.383	41.665
	50	3.723	12.500	1.022	89.558	0.417	40.762
	60	3.949	15.000	1.227	89.695	0.443	36.083
0.5	1	3.210	0.500	0.041	9.223	0.037	90.476
	3	3.319	1.500	0.123	24.962	0.104	84.407
	5	3.426	2.500	0.204	35.877	0.154	75.126
	10	3.351	5.000	0.409	57.734	0.242	59.132
	15	3.330	7.500	0.613	74.549	0.310	50.588
	20	3.466	10.000	0.818	84.412	0.366	44.715
	30	3.336	15.000	1.227	86.736	0.362	29.478
	45	3.584	22.500	1.840	91.799	0.411	22.345
	50	3.869	25.000	2.045	91.392	0.442	21.614
	60	4.003	30.000	2.454	92.042	0.461	18.766
1	1	3.326	1.000	0.082	16.424	0.068	83.473
	3	3.307	3.000	0.245	38.831	0.161	65.406
	5	3.450	5.000	0.409	60.954	0.263	64.272
	10	3.249	10.000	0.818	80.976	0.329	40.210
	15	3.328	15.000	1.227	89.990	0.374	30.508
	20	3.665	20.000	1.636	91.503	0.419	25.623
	30	3.465	30.000	2.454	93.069	0.403	16.429
	45	3.620	45.000	3.681	93.409	0.423	11.484
	50	3.751	50.000	4.090	93.986	0.441	10.776
	60	3.766	60.000	4.908	94.072	0.443	9.022

The values of % R, % Fe_M, and % H_2 utilization obtained in **Table 5.8, 5.9 and 5.10** were plotted against reduction time and is shown in **Figure 5.4**

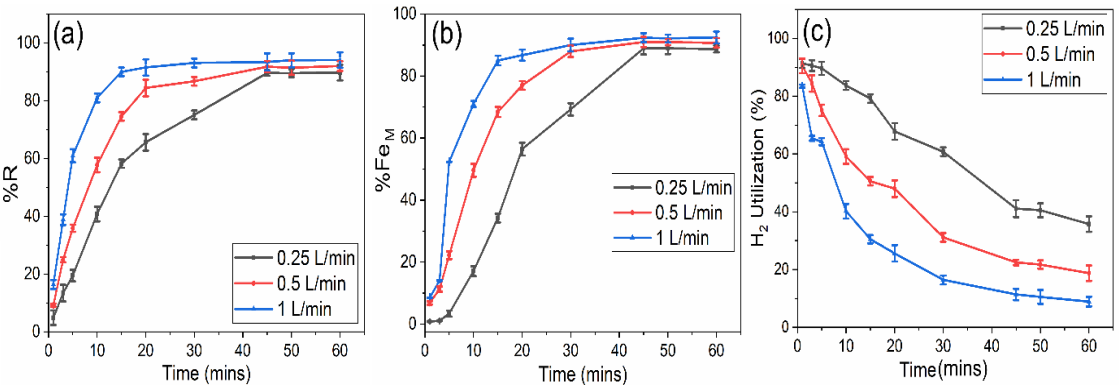

Figure 5.4 : Variation of (a) % R (b) % Fe_M (c) % H_2 utilization; with time of exposure at 900 °C

In general, the % Reduction (%R) and % Metallization (%Fe_M) values were found to increase with increase in flow rate and reduction time. However, increase in reduction time beyond 45 mins did not significantly improve the reducibility and metallization of pellets. The % H_2 utilization decreased monotonically with increased flow rates. An increase in flow rate leads to increased hydrogen gas near the pellet surface, thereby enhancing the rate of chemical reaction and increasing reducibility[103]. At 900 °C, the maximum possible %R and % Fe_M was 94.07 % and 92.45 % respectively, which was attained at a gas flow rate of 1 L/min and a reduction time of 60 mins. This was the maximum possible % R and % Fe_M obtained across all temperatures and flow rates used in this study. The %Fe_M values (92.45%) obtained are similar to those achieved with carbonaceous reductants in Section 4.2.2 of chapter 4. However, it was attained at a lower temperature and within a shorter reduction time. This underscores the advantages of utilizing H_2 as a reductant for the MMO pellets.

Temperature had a more profound effect on the reducibility of pellets with H_2 than the gas flow rate. At a gas flow rate of 1 L/min and a reduction time of 45 mins, the %R and % Fe_M increased about 10.66 % and 17.26 % respectively, when the temperature was increased from 700°C to 900 °C (**Figure 5.1 and 5.4**). Similarly, the %R and % Fe_M increased about 1.6 % and 3.8% respectively, when the temperature was increased

from 800°C to 900 °C (**Figure 5.3 and 5.4**). This increase in both the %R and the %Fe_M can be attributed to the accelerated diffusion rates of H_2 gas and increase in the rate of chemical reaction with rise in temperatures. As the temperature increases, the kinetic energy of the hydrogen molecules also rises [61]. This heightened kinetic energy increases the mobility of hydrogen molecules, and deeper penetration into the iron pellets during the reduction process is achieved [71].

On the contrary, increase in flow rate from 0.25L/min to 0.5L/min or 1L/min did not significantly improve the % R and % Fe_M values after 45 mins (**Figure 5.4**). The % R and % Fe_M achieved at a flow rate of 0.25 L/min, temperature of 900 °C, and reduction time of 45 mins are 89.5 % and 86%, respectively. At the same temperature and reduction time, the % R and % Fe_M increased slightly to 92.3% and 88.9 %, respectively, for flow rates of 0.5 L/min, which further slightly increased slightly to 93% and 92.3%, respectively, for a flow rate of 1 L/min. Though there is a minor improvement in the % R and % Fe_M by increasing the flow rate, the % H_2 utilization decreased from 41% at a flow rate of 0.25 L/min to 22.4 % at a flow rate of 0.5 L/min which further decreased to just 11.38 % at a flow rate of 1L/min, at the temperature of 900 °C and reduction time of 45 mins (**Figure 5.4c**). Thus, to avoid wastage of gas at 900 °C, a reduction time of 45 mins and a flow rate of 0.25L/min was fixed to be the optimum conditions for the reduction of the pellets by hydrogen gas. The optimum conditions yielded a % R and % Fe_M of 89.5 % and 86%, respectively, which met the industrial standards according to IS 15774[80].

The % H_2 utilization was found to increase with rise in temperature and flow rate and decrease with reduction time. The reduction reaction of iron oxides is usually hetergeneous in nature, wherein chemical reaction control and diffusion control are not independent [17]. The removal of oxygen from iron oxides happens according to:

$H_2 + O_{lattice} \Leftrightarrow H_2O$.....(5.4)

The reaction results in the separation of the oxygen from the oxide lattice, whose rate increases with increase in temperature, availability of vacant active reaction sites and concentration of gaseous reductant. Thus, initially, in the absense of any product layer, the % hydrogen utilization increases with increase in temperature as it increases the rate of chemical reaction. Increase in flow rate increseases the concentration of the gaseous reductant and thus % H_2 utilization increases.

The amount of active available vacant sites decreases with increase in reduction time (as the total amount of removable oxygen decreases with increase in time). This is the reason for the decrease in % H_2 utilization decreases with increase in reduction time.

Moreover, with increase in time at a particular temperature, the control of the reaction starts shifting to diffusion control due to formation of a product layer. The reaction front progressively shrinks uniformly for the surface. The reducing gas has to now diffuse through the product layer (whose thickness increases with increasing reduction time) to reach the reaction front. This increased resistance to diffusion of reducing gas also leads to drop in % H_2 utilization.

Since increasing the holding time beyond 45 mins led to wastage of gas without any appreciable increase in % R and % Fe_M, the focus of further investigations was limited to the time duration of 1- 45 mins.

5.2.2. Cracking and drop in CCS of pellets after reduction

It was observed that the pellets were cracking after reduction, and the severity of cracking increased with an increase in temperature and reduction time, as seen in **Figure 5.5**.

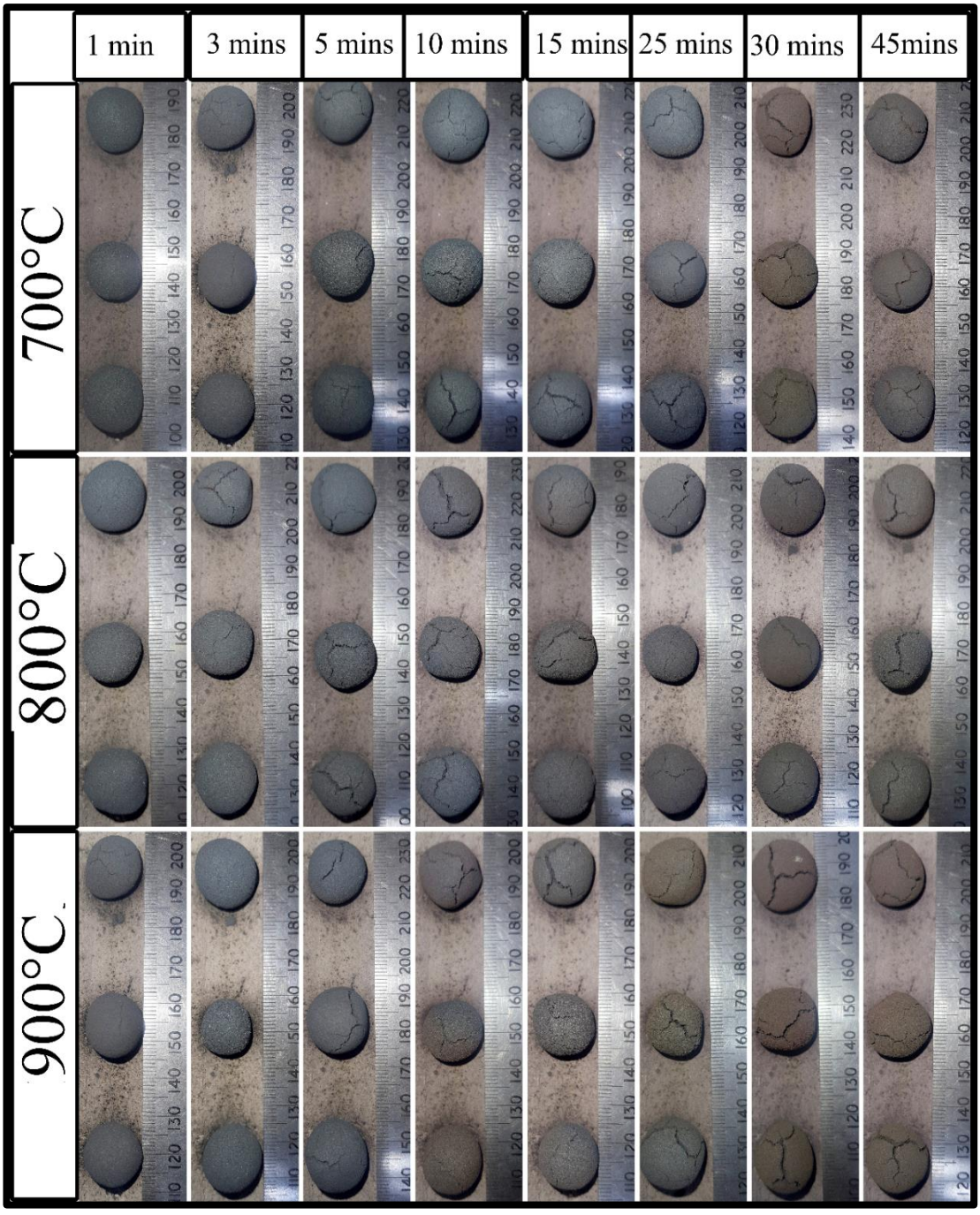

Figure 5.5: Photographs of pellets after reduction for various time-temperature combinations at a flow rate of 0.25L/min

No such cracking was observed when carbon was used as reductant (**Figure 4.1 and 4.2**). This effect was completly opposite to that reported in other studies in which

carbon reduced pellets were more prone to cracking than hydrogen reduced pellets[104, 105]. The pellets were cut into two halves and the cross sections are shown in **Figure 5.6** to investigate the nature of cracks in the pellets.

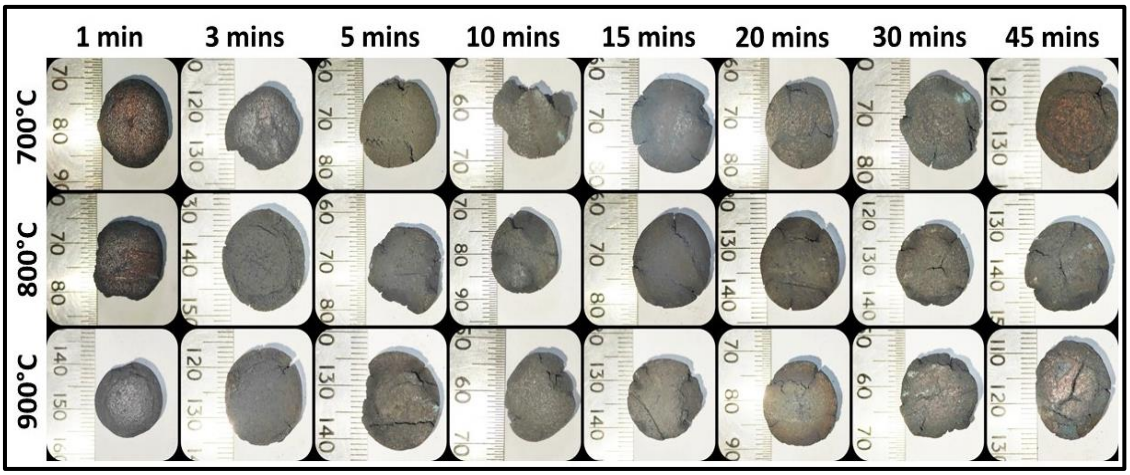

Figure 5.6: Photographs of cross section of pellets after reduction for various time-temperature combinations at a flow rate of 0.25 L/min

On examining the cross section, it was observed that the depth of cracks increased with increase in reduction time and temperature. The pellets reduced for 1 minute at any of the three temperatures did not exhibit any cracking. The cracks seem to be making their way into the core of the pellets, the length of which increased with increase in reduction time and temperature. A large central crack is visible in the pellet reduced at 900 °C for 45 mins. Cracking could lead to changes in the Compressive Strength after reduction of the pellets, which is a critical factor for use in any shaft furnace. Thus, the crushing strength (CCS) of pellets after reduction was measured according to the methods detailed in Section 2.5.2 of chapter 2 and is given in **Figure 5.7a**.

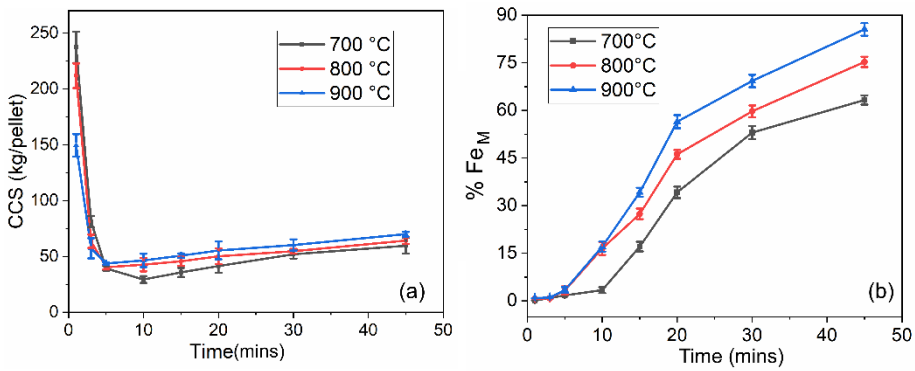

Figure 5.7: Variation of (a) CCS and (b) % Fe_M; for different time-temperature combinations at flow rate of 0.25L/min

The CCS was found to initially decrease drastically to less than 50 kg/pellet and then increase at all temperatures. The strength of pellets reduced at 800 °C and 900 °C reduced till 5 mins, and increased thereafter. However, the strength of the pellets reduced at 700 °C, decreased till 10 mins of exposure time and then increased. It can be observed from **Figure 5.7** that CCS is closely related to % Fe_M. The CCS decreased till negligible % Fe_M (**Figure 5.7b**) and then started increasing with increasing metallization. %Fe_M was less than 10% for the first 5 mins at 800 °C and 900 °C, after which CCS increased along with an increase in %Fe_M. Similarly, %Fe_M was less than 10% at 700 °C for the first 10 mins, after which CCS increased along with an increase in Metallization. Phase changes and morphological changes in the pellets due to H_2 reduction could be the cause of the cracking and change in strength of the pellets. Both of these factors are investigated in the following sections

5.2.2.1. XRD analysis

The increase in the CCS of pellets could be directly related to the increase in Metallization of the pellets. To ascertain this effect, XRD analysis of pellets reduced at 700 °C, 800 °C, 900 °C, and at a flow rate of 0.25 L/min was carried out and is presented in **Figure 5.8, 5.9 and 5.10**. After reduction for 1 minute, the primary phases are magnetite (Fe_3O_4), hematite (Fe_2O_3), Quartz (SiO_2), Chromium Iron oxide ($Fe_{1.25}Cr_{0.75}O_3$), and Aluminium Silicate (Al_2SiO_5). The transformation of hematite to magnetite in the temperature range of 700-900 °C happens according to the following reaction:

$$3\,Fe_2O_3 + H_2(g) \Leftrightarrow 2\,Fe_3O_4 + H_2O(g) \qquad \Delta G_r = \text{-91.98 KJ to -109.881 KJ} \ldots (5.5)$$

At a reduction temperature of 700 °C, Iron is visible after 15 mins (**Figure 5.8**), while it was visible from 10 mins onwards for both reduction temperatures of 800 °C (**Figure 5.9**) and 900 °C (**Figure 5.10**).

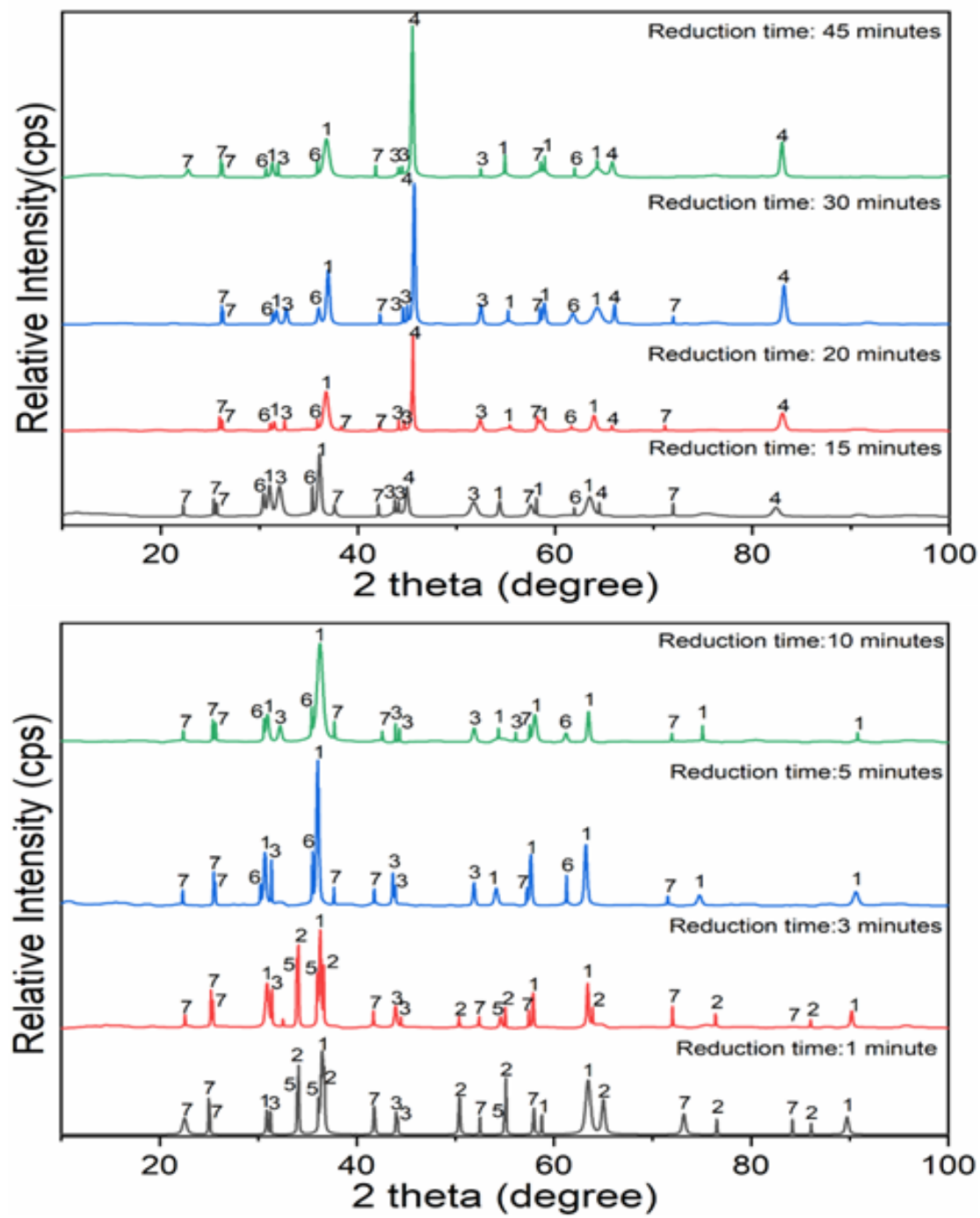

Figure 5.8: XRD analysis of pellets reduced at a flow rate of 0.25L/min for different reduction times at 700 °C

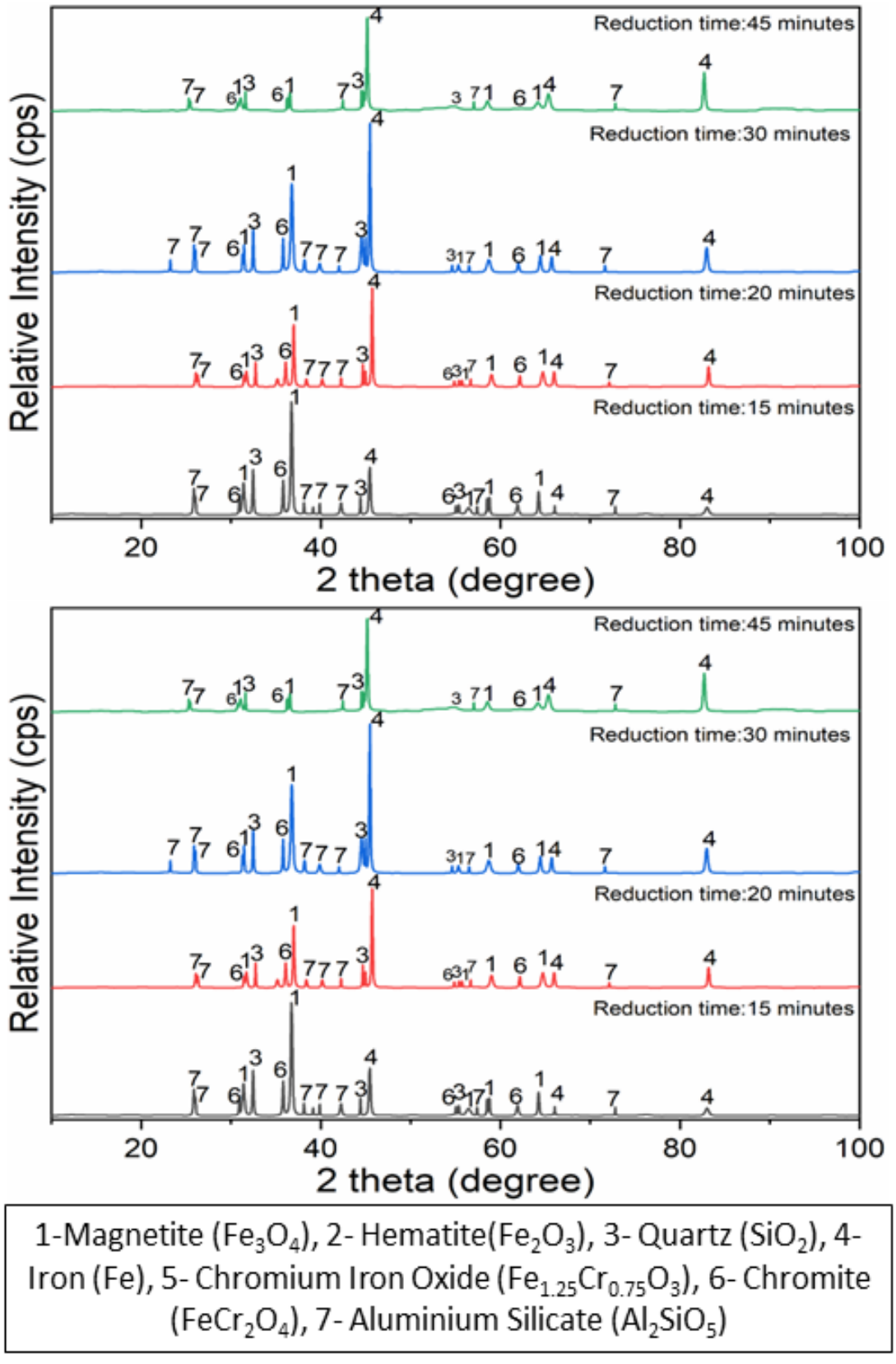

Figure 5.9: XRD analysis of pellets reduced at a flow rate of 0.25L/min for different reduction times at 800 °C

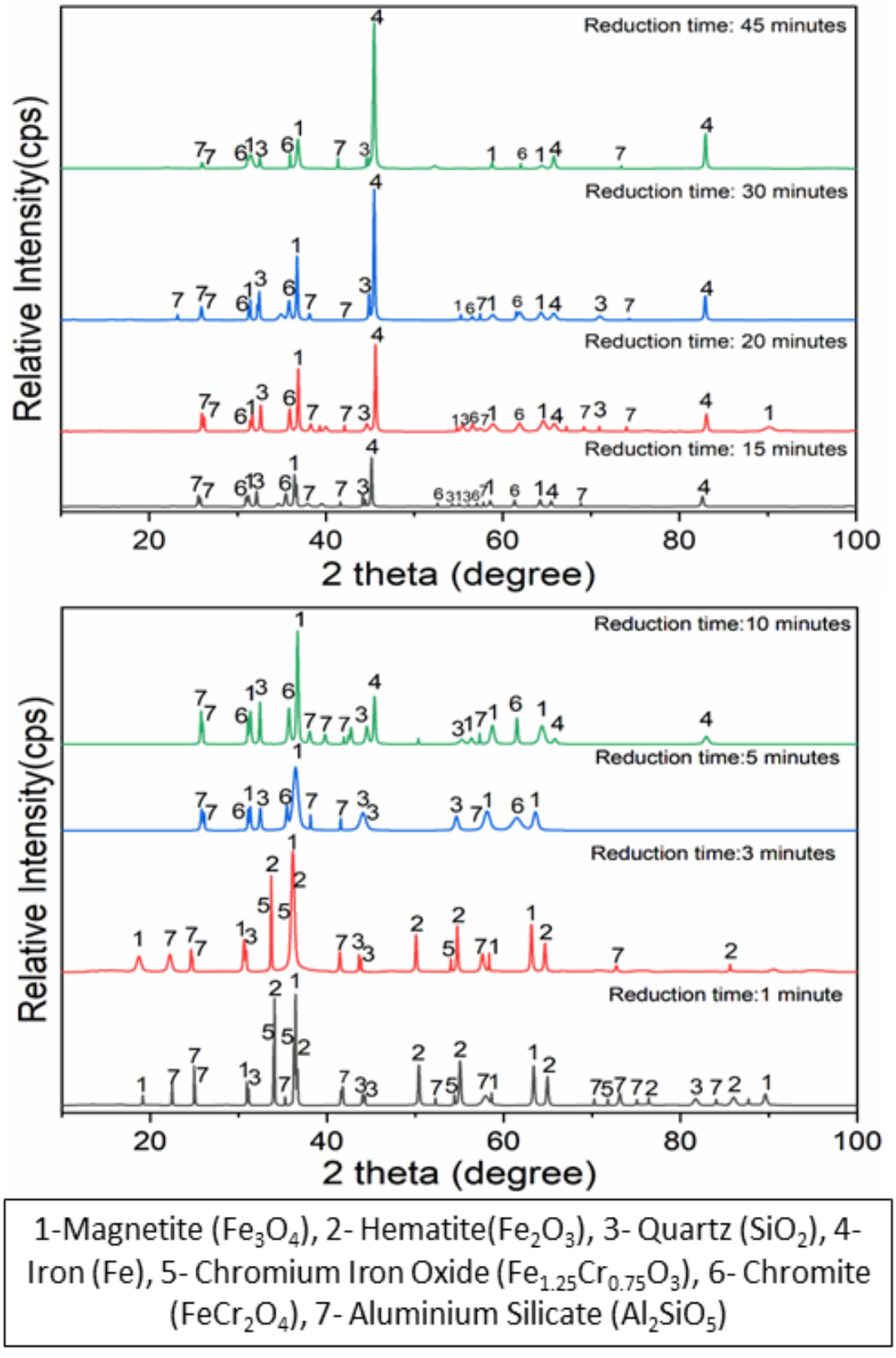

Figure 5.10:XRD analysis of pellets reduced at a flow rate of 0.25L/min for different reduction times at 900 °C

The transformation of hematite to iron in the temperature range of 700-900 °C happens according to the following reaction

$Fe_2O_3 + 3H_2(g) \Leftrightarrow 2\,Fe + 3\,H_2O(g)$ ΔG_r= -14.69 KJ to -30.68 KJ……(5.6)

As the reduction temperature is above 570 °C, this transformation usually occurs in 3 steps [102]. Initially Fe_2O_3 gets converted into Fe_3O_4 according to **eqn. 5.4**. Then Fe_3O_4 gets coverted to FeO in the temperature range of 700-900 °C as per the following reaction

$Fe_3O_4 + H_2(g) \Leftrightarrow 3\,FeO + H_2O(g)$ ΔG_r= -19.73 KJ to -30.5 KJ…….(5.7)

The FeO then gets reduced by H_2 to Fe in the temperature range of 700-900 °C according to the following reaction

$FeO + H_2(g) \Leftrightarrow Fe + H_2O(g)$ ΔG_r= 14.56 KJ to 13.14 KJ……(5.8)

Though **eqn 5.7** has a positive ΔG_r, the overall reaction shown in **eqn 5.5** has a negative ΔG_r and thus the reduction of Fe_2O_3 to Fe proceeds spontaneously in the experimenatl temperatures used in this study.

The appearance of Iron in XRD is consistent with the % Fe_M values (**Figure 5.7b**) wherein there is a sharp increase in Metallization after 10 mins onwards at both 800 °C & 900 °C; and after 15 mins at 700 °C. The transformation of hematite to magnetite leads to expansion of the pellets, which caused the reduction of strength and cracking of pellets. A similar observation of a decrease in strength has also been reported in other studies done with gases having varying ratios of CO, CO_2, H_2 and CH_4, and the sharp change in strength was attributed to the phase transformation of hematite to magnetite[72, 104-107]. The strength of pellets improved slightly after formation of metallic iron [107, 108]. However, those studies had been conducted on high-grade ores where the ratio of metal oxide phases to nonmetal oxide phases was higher. The effect

of phase transformations of the metal oxide phases on the overall strength was more when compared to low-grade ores. The amount of slag bonding is higher in the case of low-grade ores; thus, metal oxide transformations can be expected to have less influence on the overall CCS.

5.2.2.2. SEM-EDS Analysis

SEM-EDS analysis of pellets reduced at 900°C was done to investigate the morpohological changes that could have affected the CCS of reduced pellets. **Figure 5.11** shows the SEM images of MMO pellets reduced for 5 mins, 15 mins and 45 mins. The elemental analysis of the EDS points in Figure 5.11 is shown in **Table 5.11**.

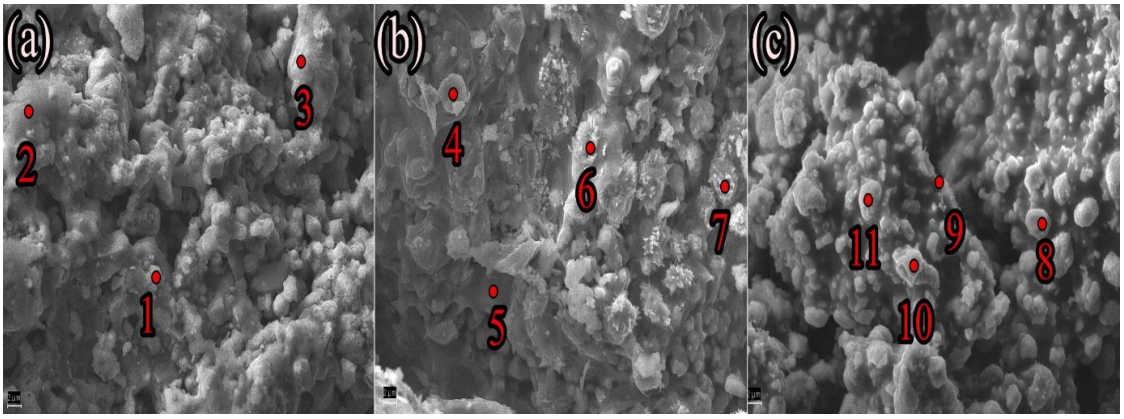

Figure 5.11: SEM images of pellets reduced at a temperature of 900 °C and a flow rate of 0.25L/min for **(a)** 5 mins**(b)**15 mins **(c)** 45 mins.

Table 5.11: Chemical compositions of the EDS points shown in Fig 5.13

Time (mins)		5			15				45			
Point No		1	2	3	4	5	6	7	8	9	10	11
Element (wt.%)	O	20.95	38.97	30.71	13.62	45.96	0	16.57	14.98	36.63	32.29	16.73
	Mg	0	1.67	0	0	0	0	0	0	2.66	1.51	0
	Al	5.22	8.71	9.39	0	12.23	0	1.29	0	14.88	7.25	0
	Si	7.06	8.10	6.76	0	11.62	0	0	0	4.74	1.78	0
	Ca	1.82	1.25	1.50	0	0	0	0	0	0	0	0
	Cr	5.26	2.95	3.32	0	4.05	1.03	0	1.59	7.14	2.91	0
	Fe	59.69	38.35	48.32	86.38	26.14	98.97	82.14	83.43	33.95	54.26	79.27

Figure 5.11 and Table 5.11 show that non-metallic oxides like SiO_2 and Al_2O_3 form brittle slag phases (point no 2), which surround the metal-rich oxide particles (points no 1&3). With progress in reduction, as seen in Figure **5.11b**, the metal oxides get reduced, leading to the generation of new phases like magnetite, wustite, and iron in the form of needles (points no 6 & 7) and spherical-shaped particles (point no 4) which occupy a larger volume than the original metal oxide (hematite), thus, leading to generation of fracture points in the brittle slag matrix. After reduction for 45 mins (**Figure 5.13c**), a large number of almost spherical particles (point no 8,11) can be seen in a slag matrix (point no 9). As the number of such spherical particles increases with an increase in reduction time (**Figure 5.13c**), the cracking intensity was found to increase with an increase in reduction time. Hydrogen reduction is usually a very fast process at high temperatures, and the entire volume of the pellets can be expected to get reduced almost simultaneously. Thus, large-scale nucleation of new phases could lead to the generation of cracks in multiple places in the slag matrix. Despite the presence of cracks, the hard metallic phase generated improves the compressive load-bearing capability of the pellets and contribute positively to the overall CCS of the pellets. As a result of which the CCS increased with an increase in metalllization. It can be observed that the presence of gangue elements might have an influence on the crushing strength of reduced iron ore pellets. The influence of the gangue elements was investigated in the next section.

5.2.3. Effect of Gangue Content on CCS and Reducibility of Pellets

It was essential to investigate the possible influence of gangue elements on the CCS and the reducibility of pellets. For this purpose, synthetic hardened pellets were made according to methods mentioned in Section 2.6.4. The prepared synthetic pellets were reduced in a pure H_2 environment at 900°C and flow rate of 0.25L/min for 45 mins.

The CCS of reduced and unreduced pellets were measured according to methods mentioned in Section 2.5.2. The variation of CCS and % R with respect to change in wt.% of gangue oxides are shown in **Figure 5.12**.

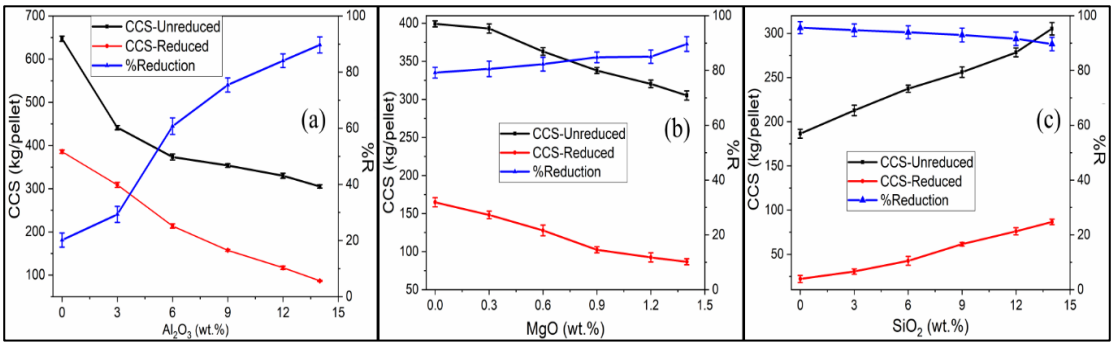

Figure 5.12: Variation of CCS of unreduced pellet, CCS of reduced pellet, and % Reduction with respect to change in **(a)** % Al_2O_3 **(b)** % MgO **(c)** % SiO_2

It can be observed in **Figures 5.12a and 5.12b** that the CCS of indurated as well as reduced pellets decreased with an increase in the amount of Al_2O_3 and MgO. On the contrary, increased SiO_2 tends to increase the CCS of both reduced and unreduced pellets (**Figure 5.12c**).Similar effect was observed in a study carried out by Yi et al wherein SiO_2 enhanced the strength and reduced RDI [105]. The influence of gangue content on pellet porosity, subsequently affecting the CCS of pellets, is evident. This relationship can be corroborated by examining the % Reduction (%R) curves presented in **Figure 5.12**. The %R of pellets exhibited improvement along with simultaneous decline in CCS (**Figures 5.12a and 5.12b)** and vice versa (**Figure 5.12c**). This inverse relationship between %R and CCS underscores the influence of pellet porosity, which is affected by gangue content. A high % R indicates higher porosity, as it facilitates better gas diffusion into the pellet structure. Conversely, lower porosity, hinders gas diffusion, resulting in reduced reducibility [17]. Hence, the observed patterns in %R and CCS in **Figure 5.12** support the idea that gangue content influences pellet porosity and subsequently CCS.

To further understand the effect of gangue on the porosity, the indurated pellets with different gangue compositions were imaged using SEM, and are shown in **Figure 5.13, 5.14 and 5.15**. Additionally, the porosity of the hardened pellets was measured according to methods mentioned in Section 2.5.3 of Chapter 2 and is shown in **Figure 5.16.** It can be observed from **Figure 5.14** that the amount of pores, i.e., porosity, increases with an increase in Al_2O_3 content. Similarly, the porosity increased with increased MgO content (**Figure 5.15**) and decreased with a rise in SiO_2 (**Figure 5.13**) content. The observed microstructures are in agreement with the experimentally obtained porosity values, as shown in **Figure 5.16**. The porosity increased with a rise in Al_2O_3 and MgO contents and declined with increasing SiO_2 content. The different products formed by the reaction of metallic oxides and gangue non-metallic oxides could be the reason for the different porosities.

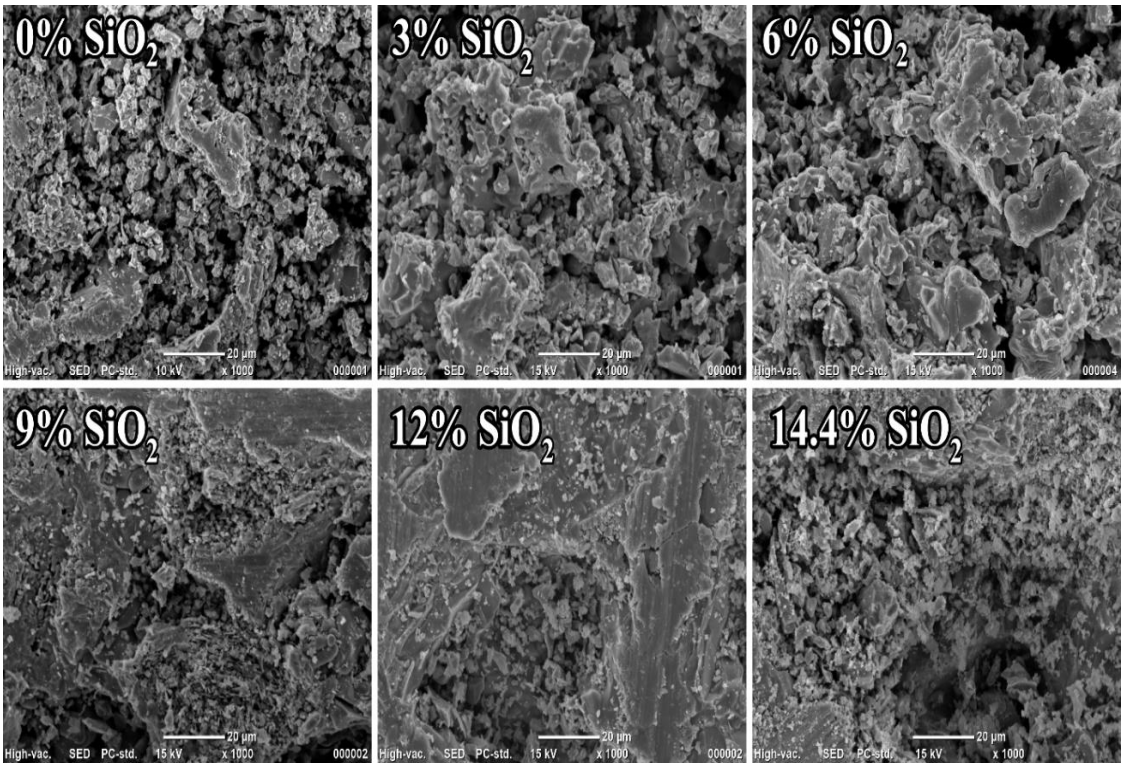

Figure 5.13: SEM images of hardened pellets depicting variation in porosity with respect to change in SiO_2 content

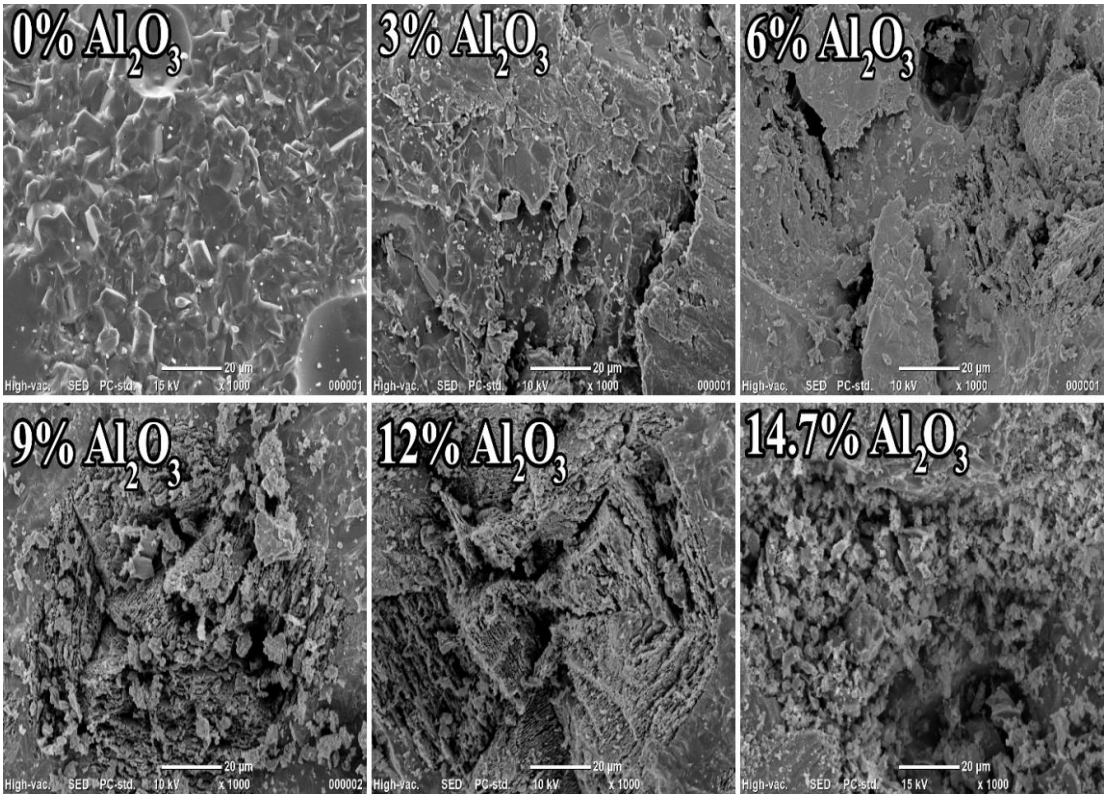

Figure 5.14: SEM images of pellets depicting variation in porosity with respect to change in Al_2O_3 content

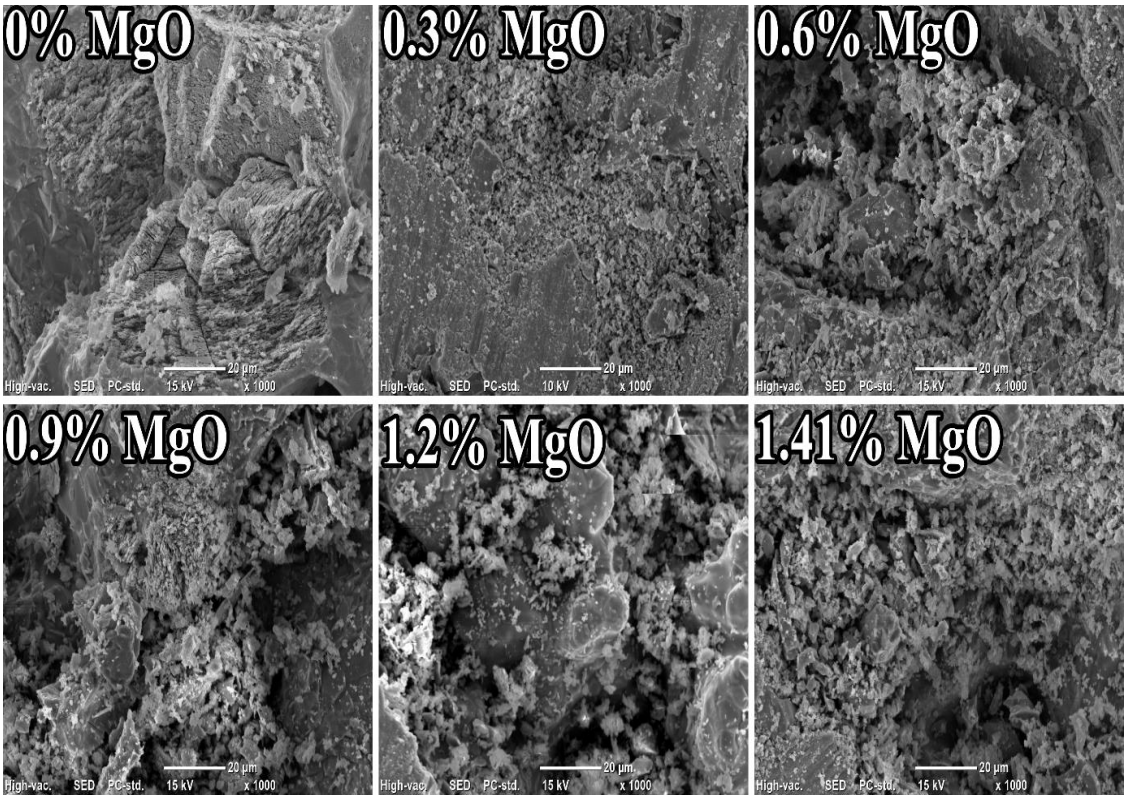

Figure 5.15:SEM images of hardened pellets depicting variation in porosity with respect to change in MgO content

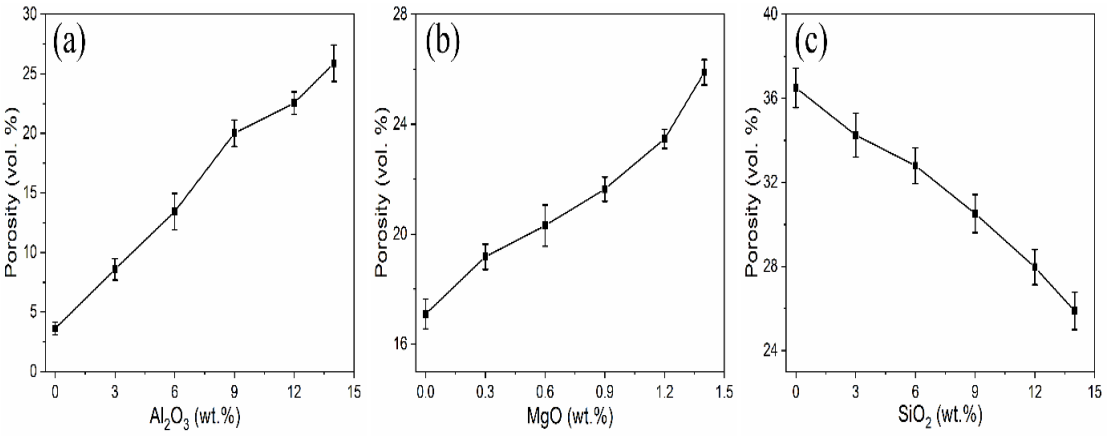

Figure 5.16: Variation of porosity with respect to changes in (a) wt.% Al_2O_3 (b) wt.% MgO (c) wt.% SiO_2

Thus, XRD analysis of the unreduced pellets containing different amounts of gangue oxides was done to determine the phases formed, as shown in **Figure 5.17.** Magnetite transformed to hematite, which usually happens whenever magnetite is indurated at higher temperatures (**eqn 3.1**)[85]. Mullite ($Al_6Si_2O_{13}$) phase formed with rise in SiO_2 content (**Figure 5.17 a, b & c**) and rise in Al_2O_3 content (**Figure 5.17 g, h & i**). Mullite phase is always formed at the induration temperatures of 1250°C used in this study according to the reaction

$$2\,SiO_2 + 3\,Al_2O_3 \iff Al_6Si_2O_{13} \qquad \Delta G_r = -33.026\ KJ \ldots\ldots\ldots\ldots\ldots\ldots (5.9)$$

This can also be confirmed from the SiO_2 - Al_2O_3 phase diagram (**Figure 5.18a**) which predicts the formation of mullite above 1250 °C [109, 110]. Magnesioferrite ($MgFe_2O_4$) phase is obtained when MgO content is increased (Figure 5.19 d, e & f). $MgFe_2O_4$ is formed at 1250 °C [93, 111] according to the following reaction

$$2\,MgO + 3\,Fe_2O_3 \iff MgFe_2O_4 \qquad \Delta G_r = -15.19\ KJ \ldots\ldots\ldots\ldots\ldots\ldots (5.10)$$

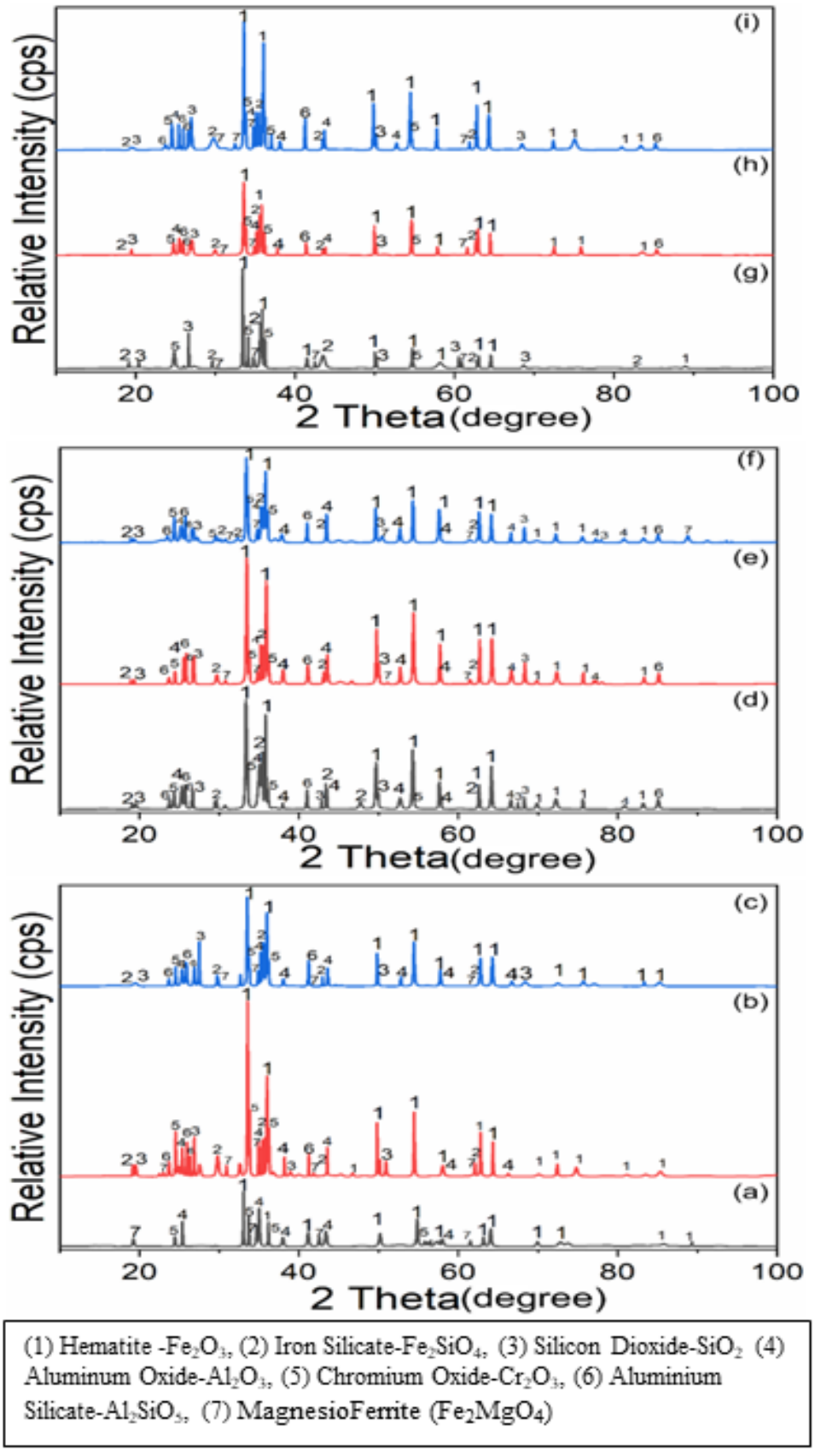

Figure 5.17: XRD analysis of pellet containing (a)0 wt.% SiO_2 (b)6 wt.% SiO_2 (c)12 wt.% SiO_2 (d)0 wt.% MgO (e) 0.6 wt.% MgO (f) 1.2 wt.% MgO (g) 0 wt.% Al_2O_3 (h)6 wt.% Al_2O_3 (i) 12 wt.% Al_2O_3

During induration, the increase in CCS also occurs due to slag bonding provided by the melt phases. In the XRD patterns in **Figure 5.17**, no such phase was obtained that could melt at the induration temperature of 1250 °C used in this study. However, B_2O_3 present in the colemanite binder used in the study always forms a low melting borosilicate phase in association with SiO_2. B_2O_3 reacts easily with SiO_2 to form a liquid melt phase as shown in the B_2O_3-SiO_2 phase diagram (**Figure 5.18b**) [112]. As the amount of melt phase was low it was not detected in XRD. This melt phase was absent in the 0 wt.% SiO_2 pellets. Thus, the CCS of unreduced pellets was lowest at 186.48 kg/pellet (Figure 5.14c) and porosity was highest at 36.49 vol.% (**Figure 5.18c**) for the 0 wt.% SiO_2 pellets. The only bond in those pellets could be due to the diffusion bonded newly formed Fe_2O_3 grains [113]. The amount of melt phase increased with the rise in SiO_2 content in pellets. Thus, the area occupied by the melt phase increased which increased the amount of slag bond and CCS of pellets. The melt also filled up a larger number of pores and reduced porosity. The most significant variation in CCS of unreduced pellets was observed when the amount of Al_2O_3 was varied in the pellets (**Figure 5.12a**). In 0 wt.% Al_2O_3 pellets, the porosity was lowest at 3.61 vol.% and CCS was highest at 647.13 kg/pellet. The melt phase in 0 wt.% Al_2O_3 comprised of only B_2O_3 and SiO_2. Upon addition of Al_2O_3 to the pellet, the viscosity of the melt increased. Hence the area of pellet occupied by the melt phase and the subsequent amount of slag bond decreased with rise in Al_2O_3 content. The number of pores filled decreased and the CCS increased as result of reduction in amount of slag bond. The reverse effect of Al_2O_3 on melt phase is observed in the case of MgO (**Figure 5.12b**). MgO being a network breaker decreases the viscosity of the melt phase. Though the area occupied increased due to increase in flowability of the melt phase, the thickness of the melt phase and the subsequent strength of slag bond decreased. The CCS dropped slightly and porosity increased

slightly. However, as the variation in MgO content is not as high as that of Al_2O_3 and SiO_2, CCS and porosity are not affected much.

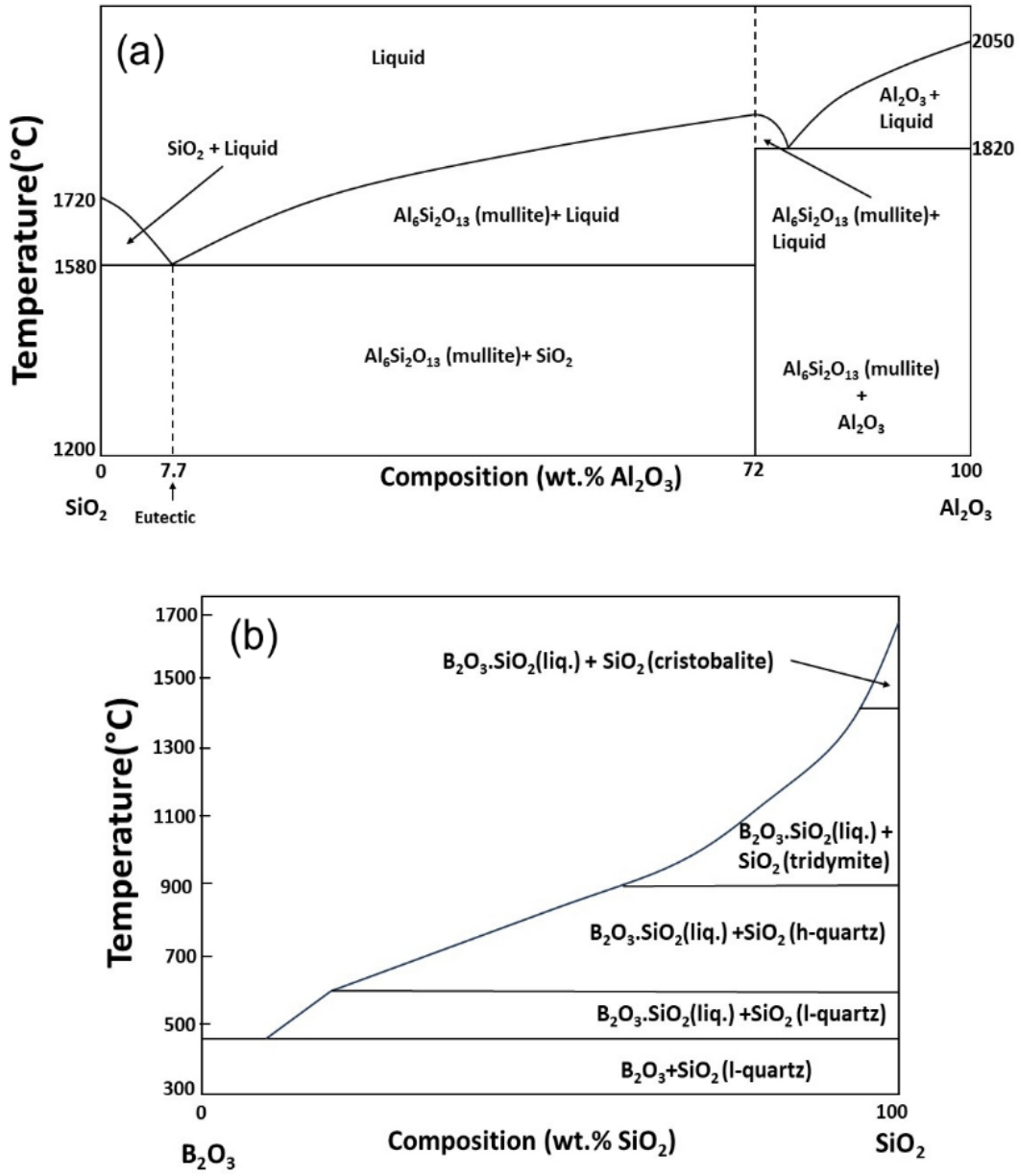

Figure 5.18: (a) SiO_2-Al_2O_3 phase diagram (adapted from Sarkar, Callister [109,110])
(b) B_2O_3- SiO_2 phase diagram [112]

As observed from **Figure 5.11**, the brittle slag phases encompassed the metallic oxide phases in the pellets. The porosity of the brittle phases had a prominent role in controlling the reducibility and the subsequent drop in the CCS of pellets. The rapid

generation of new phases (having a volume larger than initial metal oxides) in the slag phase due to the fast reduction kinetics obtained using H_2 gas led to a surge in internal stress inside the pellet. Although an increase in porosity led to an improvement in %R, there was also a drop in CCS and vice versa (**Figures 5.12 and 5.16**). Too low a porosity led to a gradual drop in CCS and a low reduction degree, and too high a porosity gave an excellent reduction degree but a rapid decline in CCS—for instance, 0 wt.% Al_2O_3 pellets, which had a porosity of just 3.6 vol.% (**Figure 5.16a**), gave a poor %R and drop in CCS after reduction of 20.16 % and 25%, respectively (**Figure 5.12a**). But 0 wt.% SiO_2 pellets, which had a porosity of 36.49 vol.% (**Figure 5.16c**), gave an excellent % R and rapid drop in CCS after reduction of 95.62 % and 88%, respectively (**Figure 5.12c**). As the voidage and the amount of newly formed phases was more in 0 wt.% SiO_2 pellets, the drop in CCS was more severe. Thus, variation in gangue oxides controlled the porosity of pellets, which in turn affected the reducibility of pellets and subsequent drop in CCS after reduction. Therefore, an optimum porosity, brought by proper control of gangue oxides, must be maintained to obtain good reducibility without significantly sacrificing CCS after reduction.

5.3. Conclusions

This chapter presents the effect of reduction time, temperature, and H_2 gas flow rate on reduction of pellets made from low-grade multimetallic ore. The effect of the gangue oxides (MgO, Al_2O_3, SiO_2) on the CCS and H_2 reducibility of the pellets has also been studied by reducing synthetic pellets having varying amounts of the gangue oxides.

- A % R of more than 90 % and % Fe_m of more than 85% after about 20 mins of reduction time at a reduction temperature of 900°C and gas flow rate of 1 L/min was achieved, which is in line with IS 15774. This shows that hydrogen reduction

can be a feasible option for processing low-grade iron ores as the reduction times can be significantly reduced compared to carbothermic reduction.

- The low % H_2 utilization and the high cost of H_2 gas led to the selection of optimum process parameters of 45 mins reduction time, 900°C reduction temperature, and 0.25 L/min flow rate. The optimum conditions produced a %R of ~90 %, a % Fe_M 89%, and a % H_2 utilization of more than 40%.
- At the optimized reduction parameters, pellet cracking was observed, and pellets' CCS dropped drastically from 285 kg/pellet (hardened pellet) to 60 kg/pellet after reduction, which was just above the limit specified in standards. SEM studies indicated that the cracking of pellets and a drop in CCS were due to the large-scale nucleation of reduced phases in the form of needles and spherical particles in a brittle slag phase. Such a sharp drop in the CCS of low-grade iron ore pellets in the shaft furnace could result in the disintegration of pellets during reduction.
- The porosity & drop in CCS of pellets after reduction increased with the addition of Al_2O_3 & MgO and decreased with the rise in SiO_2 content. Complete removal of SiO_2 led to a drastic deterioration in CCS after reduction from 186.48 kg/pellet to 22 kg/pellet. On the other hand, the complete removal of Al_2O_3 produced a porosity of just 3.6 vol.% and a % Reduction of 20%. These observations implied that despite the negative effect of gangue oxides on the productivity of furnaces, they should not be eliminated entirely when low-grade iron ore pellets are reduced by hydrogen.
- B_2O_3 present in the colemanite binder formed a melt phase with SiO_2. Increase in SiO_2 content increased the amount of melt phase and depreciated the porosity of pellets from 36.5 vol.% to 25.8 vol.%. SEM studies also confirmed that the porosity of pellets dropped with a rise in SiO2 content and improved with a rise in Al_2O_3 content. An increment in Al_2O_3 content increased the viscosity and reduced the

flowability of the borosilicate melt phase. As a result, the porosity of the pellets improved from 3.6 vol.% to 25.8 vol.%. Thus, proper control of the gangue oxide content in low-grade ores could maintain the porosity and CCS after reduction of H_2-reduced pellets without compromising reducibility.